RAPID COMMUNICATIONS

PHYSICAL REVIEW B VOLUME 52, NUMBER 4 15 JULY 1995-II

Nanocrystalline Ge filaments in the pores of a mesosilicate

R. Leon*
Center for Quantized Electronic Structures, University of California, Santa Barbara, California 93106

D. Margolese and G. Stucky
Chemistry Department, University of California, Santa Barbara, California 93106

P. M. Petroff
Materials Department and Electrical and Computer Engineering Department, University of California, Santa Barbara, California 93106

(Received 16 February 1994; revised manuscript received 25 April 1995)

Direct imaging showing pore filling of a mesopore (MCM-41) by a semiconductor has been achieved by transmission-electron microscopy (TEM). Ge was deposited using vapor-phase epitaxy where the mesopore wall hydroxyls acted as anchor points to seed the nucleation of semiconductor clusters in the mesosilicate channels. Dark-field TEM micrographs with diffraction contrast originating exclusively from germanium show sections of Ge crystallites taking the shape and periodicity of the mesosilicate, indicating that the deposited semiconductor can fill the hexagonal pores. This result shows promise for the use of mesopores as hosts for semiconductor quantum wire structures.

The idea of using zeolites, molecular sieve lattices for the growth of semiconductor quantum dots and wires, has been proposed,[1,2] and some success has been achieved in the loading of Ge,[3] GaP and CdS in zeolite *Y*,[4] and PbI_2 in zeolite *A*.[5] These high-dielectric aluminosilicate hosts offer high packing densities, spherically shaped voids, and channels in periodic arrays.[6] One of the main limitations of these materials is the small pore sizes available, with the upper limit of 13 Å diameter (zeolite *Y*).

The recent discovery (synthesis) of a new class of mesoporous materials opens possibilities using ordered silicate arrays as hosts for quantum semiconductor structures of low dimensionality. These materials are formed by an inorganic/organic liquid-crystal templating mechanism, where regular arrays of uniform channels are created in which the silicate materials form inorganic walls between ordered surfactant micelles.[7–10] MCM-41, the mesoporous material used in this work, has columnar periodic hexagonal pores separated by 8–9-Å walls. One of the several advantages these materials offer is flexibility in pore diameter, which can be varied by changing the alkyl chain length of the surfactant used in their synthesis. The range in pore sizes (15–100 Å) is ideally suited for the formation of semiconductor quantum structures, and the available packing density for quantum wires is very high. Recent reports demonstrating the feasibility of thicker framework walls using a neutral templating route[11] are also encouraging for quantum wire applications. The other advantage of mesopore use over the self-assembled methods recently developed[12,13] is better size uniformity and an inherent preordering of the densely packed array.

Recent optical measurements of GaAs deposited on MCM-41 has shown blueshifts[14] in luminescence, presumably due to quantum confinement effects. However, it has also been observed that the small GaAs crystallites deposit on the surface of MCM-41, and evidence for pore filling is ambiguous from optical measurements. Quantum confinement can be produced by free-standing semiconductor nanocrystals surrounded by their own oxides,[15–17] so nanocrystals outside the mesosilicate framework could produce a blueshift as well. These mesoporous materials cannot yet be obtained in epitaxial form, and the orientation of the mesosilicate crystallites is random. This impedes some of the optically relevant measurements that could indicate two-dimensional confinement, such as polarization effects.[18]

In this work, an unambiguous structural technique has been used to image Ge filaments in the pores of MCM-41. This method makes use of the vast difference between lattice parameters for the semiconductor and its mesosilicate host. The different scales in the corresponding diffraction patterns allow isolation of diffracted beam(s) coming only from the semiconductor, and dark-field TEM images where Ge is the only contributor to the contrast can be formed.

The mesosilicate samples were prepared after the calcination[7–10] that removes the organic molecules included in the mesopore channels from the templating process. These samples were thermally dehydrated under vacuum at 150 °C for 2 h. 5–40 Torr digermane (Ge_2H_6) gas was subsequently introduced over the mesopore at room temperature. The samples were heated to 100 °C for 12–96 h, and to 250 °C for 4 h. Evacuation removed residual Ge_2H_6 and H_2 gases. Annealing in static vacuum at 500 °C for 1–2 h followed.

The calcination process leaves behind hydroxyls on the inner channel surfaces to which a variety of chemical species can be attached via an elimination reaction.[19,20] With digermane, substitution at the wall occurs with the elimination of H_2(g). Subsequent reaction in the presence of digermane at elevated temperatures leads to condensation and pore filling with Ge.

TEM samples were prepared by adhering a large number of crystallites of reacted material onto a holey carbon film on a Cu grid. A 200 FX JEOL TEM operated at 200 keV was used. Electron-diffraction patterns were obtained for both the mesoporous silicate framework and the semiconductor.

The hexagonal mesoporous silicate (MCM-41) used in this work produces two basic types of diffraction patterns, as well as two types of lattice images. The diffraction pattern

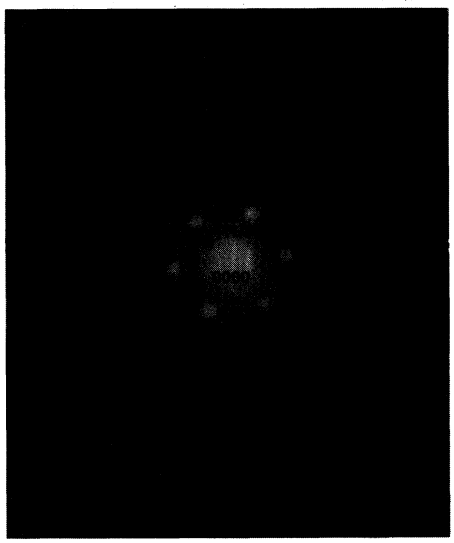

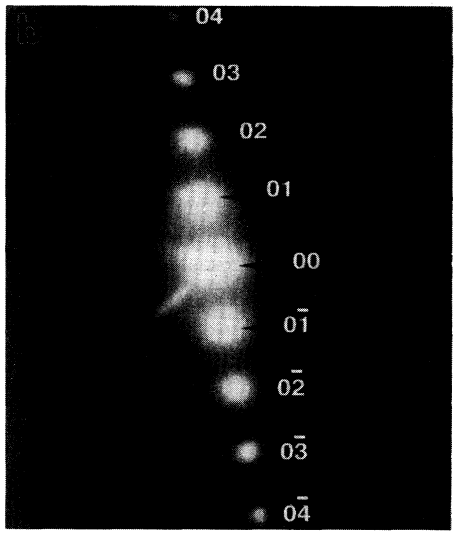

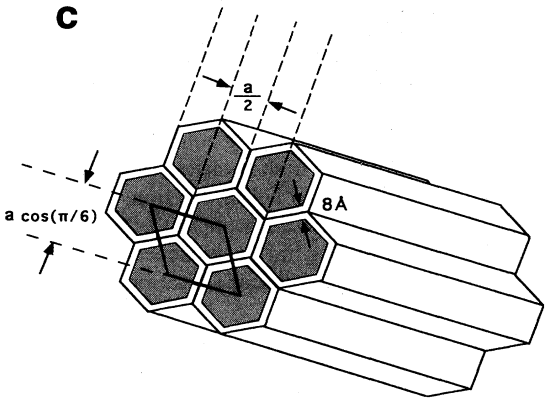

FIG. 1. Diffraction spots obtained from the mesosilicate MCM-41 used as host structure for Ge nanocrystals. The indexed diffraction pattern obtained (a) along the (0001) zone axis, and (b) normal to the hexagonal axis and parallel to two of the hexagonal tube side walls, giving d spacing of $a/2=25$ Å. (c) Diagram of an MCM-41 crystallite showing the different possible orientations that produce the lattice images shown in Figs. 4–6, as well as the diffraction patterns shown in (a) and (b).

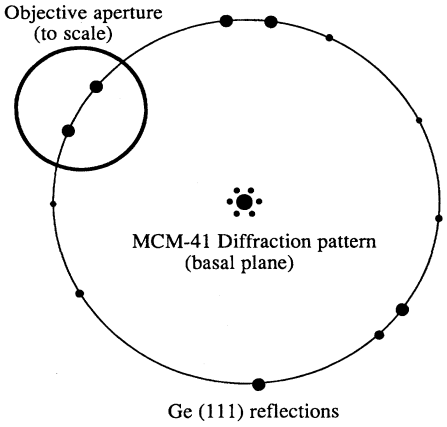

FIG. 2. Diagram showing a comparison of the relative spacings in the diffraction patterns obtained with MCM-41 crystals and the first (111) ring pattern from the germanium crystallites. The relative size of the objective aperture is also shown. Dark-field imaging was obtained with the appropriate beam tilt so diffraction spots from the mesoporous material did not contribute to the contrast seen in Figs. 4(b), 4(c), 5(b), and 6(a).

shown in Fig. 1(a) is obtained by viewing the crystallite along the axis of the hexagonal pores. This gives a [0001] pattern with sixfold symmetry. The lattice image is also hexagonal, as shown in Fig. 4(a). The lattice parameter of the mesopore was determined to be 50 ± 3 Å. A wall thickness of 8–9 Å was obtained by taking the differences between lattice spacings given by electron beam and x-ray diffraction and the average pore diameter as determined by N_2 BET (Brunaver-Emmett-Teller) measurements[9] and also by x-ray modeling.[21]

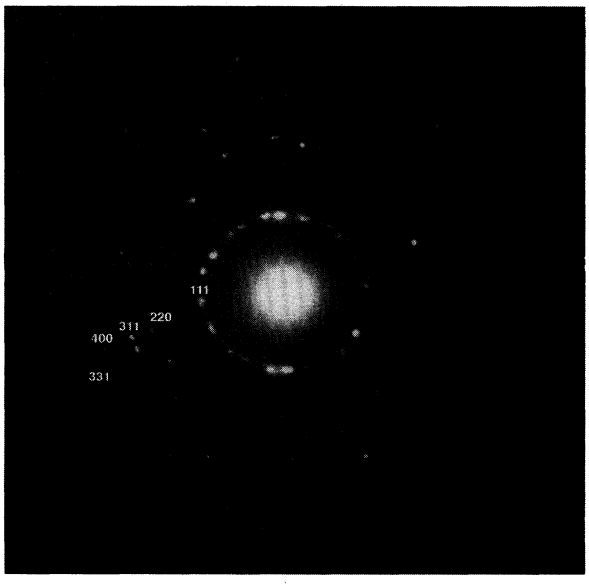

FIG. 3. Diffraction ring pattern obtained from Ge nanocrystals at several orientations in the MCM-41 framework. For randomly oriented particles and a specific beam direction, (hkl) diffracted beams will lie in a cone centered on the incident-beam direction producing a series of concentric rings each one corresponding to a set of $\{hkl\}$ reflections, as indexed here. The diffraction spots from the mesopore cannot be resolved from the transmitted beam in this figure.

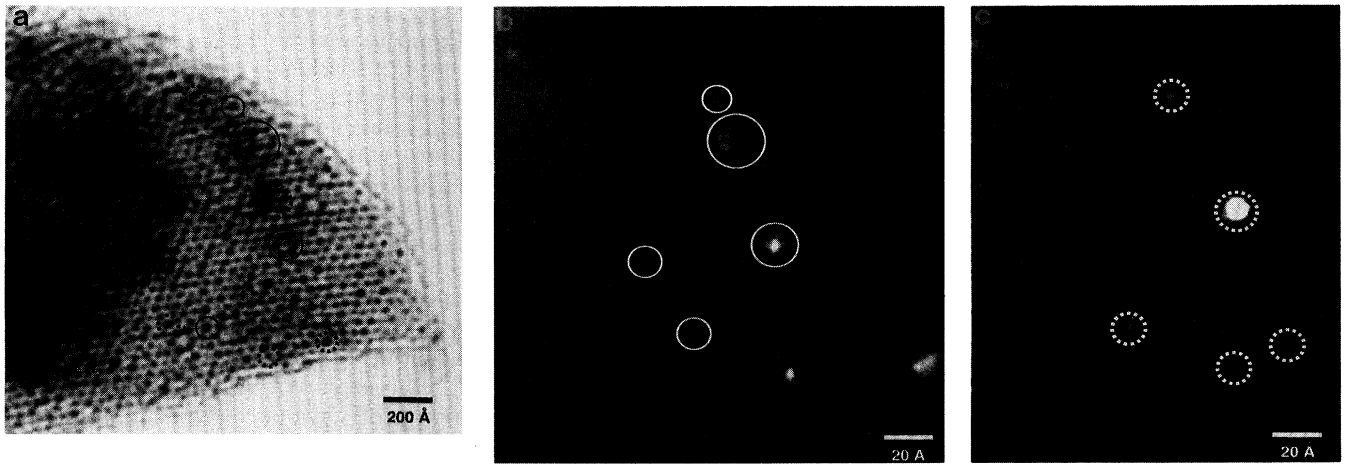

FIG. 4. (a) Phase contrast TEM micrograph obtained in axial bright-field imaging conditions shows the hexagonal framework of MCM-41. The Ge can be seen in some of the pores showing darker contrast due to stronger diffraction of the Ge crystals. (b) and (c) show axial dark-field images exhibiting contrast solely from Ge reflections chosen with two positions for the objective aperture (with some amorphous space included). The indicators show the corresponding places for the different imaging conditions.

When the crystallites are viewed normal to the hexagonal pore axis, a one-dimensional diffraction pattern results. Such a diffraction pattern is shown in Fig. 1(b). Figure 1(c) shows a diagram of the mesopore structure used. There are two possible d spacings, depending on the orientation, as illustrated in the diagram. These can be either half the lattice parameter $a/2$, or $a[\cos(\pi/6)]$. The lattice images resulting with the structure viewed normal to the pore axis consist of regularly spaced lines.

Ge is a diamond cubic semiconductor with a 5.6580-Å lattice parameter. Since Ge and MCM-41 have widely different d spacings, their corresponding diffraction patterns are also on different scales. Figure 2 is a schematic illustration comparing the relative sizes of diffraction spacings from an MCM-41 crystallite aligned along the [0001] zone axis and a few Ge crystallites at different orientations. The diagram indicates the two different scales in diffraction patterns calculated and measured for both materials. Diffraction spots from Ge crystallites are seen in the MCM-41 samples subjected to the described reaction with Ge_2H_6. Selected area diffraction gave spotty ring patterns, as expected from several nanocrystals at different orientations. Figure 3 shows a diffraction pattern obtained from mesosilicate crystals that had been reacted with digermane. The spacings within the different rings in Fig. 3 correspond to the known d spacings for Ge, and these are indexed in the figure.

Dark-field operating conditions were used for imaging Ge crystallites without contribution from the MCM-41 lattice. This was done by tilting the electron beam such that one of the spots appearing in the ring pattern was aligned with the optical axis (sometimes, more than one reflection from the Ge nanocrystals can be included within the objective aperture). The image contrast in dark fields comes exclusively from the Ge crystallites giving rise to the reflections contained in the arc, cut by the objective aperture used (this is illustrated in Fig. 2). This can be done because diffraction spots from the mesosilicate are very close to the optical axis at 130-cm camera length. The use of the objective aperture and the tilt blocks out any contribution to the image from the MCM-41 lattice. The possibility of double diffraction from the MCM-41 lattice giving rise to satellite spots has been excluded in this case. Numerous Ge-containing MCM-41 crystallites have been observed in diffraction mode, using camera lengths that permitted observation of both types of reflections, and double diffraction from the mesoporous material has never been observed. This is not surprising given the weakly diffracting nature of most mesosilicate lattices.

Figures 4 and 5 show both axial bright-field and dark-field sets of images of the same areas in the crystallite. These figures show the hexagonal framework at different orientations. In Fig. 5, the hexagonal pores are viewed from the side, giving the appearance of a layered structure. In this orientation, the one-dimensional diffraction pattern shown in Fig. 1(b) is produced. In Fig. 4 the zone axis is parallel to the sixfold hexagonal axis. In bright field, we see contributions from both the Ge crystallites and the mesoporous material. In dark field, several reflections from spots in the ringlike diffraction patterns originating from Ge are used to create different dark-field images. The areas shown enclosed by circles in Fig. 4 indicate the same areas viewed in bright and dark field. Two different dark-field tilts are shown so that contrast from Ge crystallites at different orientations can be seen.

In Fig. 5 the hexagonal tubes are oriented perpendicularly to the beam, so the image shows filaments. The spacing between the filaments in Fig. 5(b) is half of the measured lattice spacing for the MCM-41 framework. In Fig. 5(a) the contrast in dark field is enhanced due to a rotational moiré[22] effect. The image arises from the superposition of rotated Ge loaded MCM-41 crystallites. This has an enlarging effect apparent in the dark-field micrograph. A moiré pattern with two rotated crystals of equal spacings (confirmed from the bright-field images) will have moiré lines approximately perpendicular to the crystal lattice planes and an effective spacing given by

$$D = d/[2\ \sin(\beta/2)] \sim d/\beta,$$

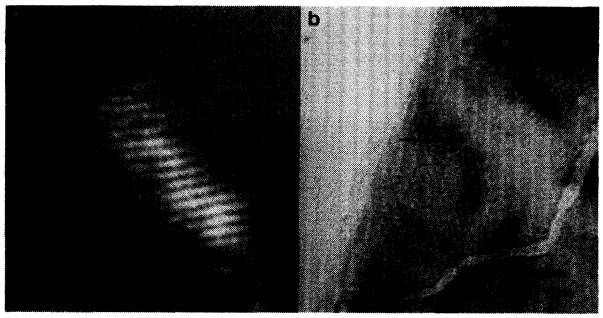

FIG. 5. (a) Dark field TEM micrograph where contrast is enanced due to moiré fringes. The smaller MCM-41 d-spacing in this orientation (25 Å) can also be seen normal to the larger moiré fringes. (b) Bright-field TEM micrograph of the same area as (a).

where β is the angular rotation between the lattice planes and d is the lattice spacing at the given orientation (25 Å in this case). In Fig. 5, β corresponds to $\sim 37°$.

The periodicity of the images in dark field has been found to correspond to the periodicity of the mesoporous lattice in many dark-field images. This indicates that the segments showing Ge contrast are indeed segments of Ge filaments or wires filling the tubular MCM-41 channels.

Even though some of the Ge filling might be missed also from the technique, it is most likely that, as seen in Figs. 4 and 5, only portions of the mesopore tubes are filled with Ge. The amount of digermane used in the reaction was insufficient to produce enough crystalline Ge to fill all the pores available in the sample. Also, some of the wall hydroxyls were left intact after reaction with the digermane so the reaction on the wall was not complete throughout all the mesopore channels. Subsequent reaction to promote filling may then just fill those sites that had been nucleated. This is the first report, to the best of our knowledge, on any success involving pore filling with a semiconductor, and future directions will involve research to achieve more complete semiconductor loading.

To conclude, evidence of Ge confined in the hexagonal pores of MCM-41 has been shown, demonstrating the feasibility of pore filling of mesoporous materials with a semiconductor. The possibilities for this alternative fabrication technique to make quantum wire and dot arrays of high packing density could have significant technological impact. Rendering these materials epitaxial in order to make the processing compatible with device fabrication technology should motivate future challenges.

This research was supported by the NSF Science and Technology Center QUEST (DMR Grant No. 91-20007). The authors would also like to thank D. Kumar and V. Srdanov for stimulating discussions and R. Egan for critical reading of the manuscript.

*Department of Electronic Materials Engineering, Research School of Physical Sciences and Engineering, Australian National University, Canberra, Australian Capital Territory, 0200 Australia

[1] G. Stucky and J. Mac Dougall, Science **247**, 669 (1990).

[2] Y. Wang and N Herron, J. Phys. Chem. **91**, 257 (1987).

[3] S. Tomiya, P. M. Petroff, D. Margolese, V. I. Srdanov, G. Stucky, and Y. Zhang, in *Nanophase and Nanocomposite Materials*, edited by S. Komarneni, J. C. Parker, and G. J. Thomas, MRS Symposia Proceedings No. 286 (Materials Research Society, Pittsburgh, 1993), p. 353.

[4] N. Herron, Y. Wang, M. Eddy, G. D. Stucky, D. E. Cox, K. Moller, and T. Bein, J. Am. Chem. Soc. **111**, 530 (1989).

[5] Y. Nozue, Z. K. Tang, and T. Goto, Solid State Commun. **76**, 531 (1990).

[6] D. W. Breck, *Zeolite Molecular Sieves* (Krieger, Malabar, FL, 1984); R. M. Barrer, *Zeolites and Clay Minerals as Sorbents and Molecular Sieves* (Academic, New York, 1978).

[7] C. T. Kresge, M. E. Leonowicz, W. J. Roth, J. C. Vartuli, and J. S. Beck, Nature (London) **359**, 710 (1992).

[8] J. S. Beck, J. C. Vartuli, W. J. Roth, M. E. Leonowicz, C. T. Kresge, K. D. Schmitt, C. T-W. Chu, D. H. Olson, E. W. Sheppard, S. B. McCullen, J. B. Higgins, and J. L. Schlenker, J. Am. Chem. Soc. **114**, 10 834 (1992).

[9] A. Monnier, F. Schuth, Q. Huo, D. Kumar, D. Margolese, R. S. Maxwell, G. D. Stucky, M. Krishnamurty, P. Petroff, A. Firouzi, M. Janicke, and B. F. Chmelka, Science **261**, 1299 (1993).

[10] Q. Huo, D. I. Margolese, U. Ciesla, P. Feng, T. E. Gier, P. Sieger, R. Leon, P. Petroff, F. Schuth, and G. D. Stucky, Nature (London) **368**, 317 (1994).

[11] P. T. Tanev and T. J. Pinnavaia, Science **267**, 865 (1995).

[12] D. Leonard, M. Krishnamurthy, C. M. Reaves, S. P. Denbaars, and P. M. Petroff, Appl. Phys. Lett. **63**, 3203 (1993).

[13] R. Leon, P. Petroff, D. Leonard, and S. Fafard, Science **267**, 1966 (1995).

[14] V. I. Srdanov, I. Kamber, C. M. Reaves, S. P. DenBaars, and G. D. Stucky (unpublished).

[15] W. A. Saunders, P. C. Sercel, H. A. Atwater, K. J. Vahala, and R. C. Flagan, Appl. Phys. Lett. **60**, 950 (1992).

[16] H. Uchida, C. J. Curtis, P. V. Kamat, K. M. Jones, and A. J. Nozik, J. Phys. Chem. **96**, 1156 (1992).

[17] W. L. Wilson, P. F. Szajowski, and L. E. Brus, Science **262**, 1242 (1993).

[18] L. Borotheau, A. Izrael, J. Y. Marzin, R. Azoulay, V. Thierry-Mieg, and F. R. Ladan, Appl. Phys. Lett. **61**, 3023 (1992).

[19] D. Margolese, V. Srdanov, R. Leon, P. Petroff, and G. Stucky (unpublished).

[20] D. Margolese, Ph.D. dissertation, University of California at Santa Barbara, 1995.

[21] A. Monnier and G. Stucky (unpublished).

[22] R. Gevers, Philos. Mag. **7**, 1681 (1962).

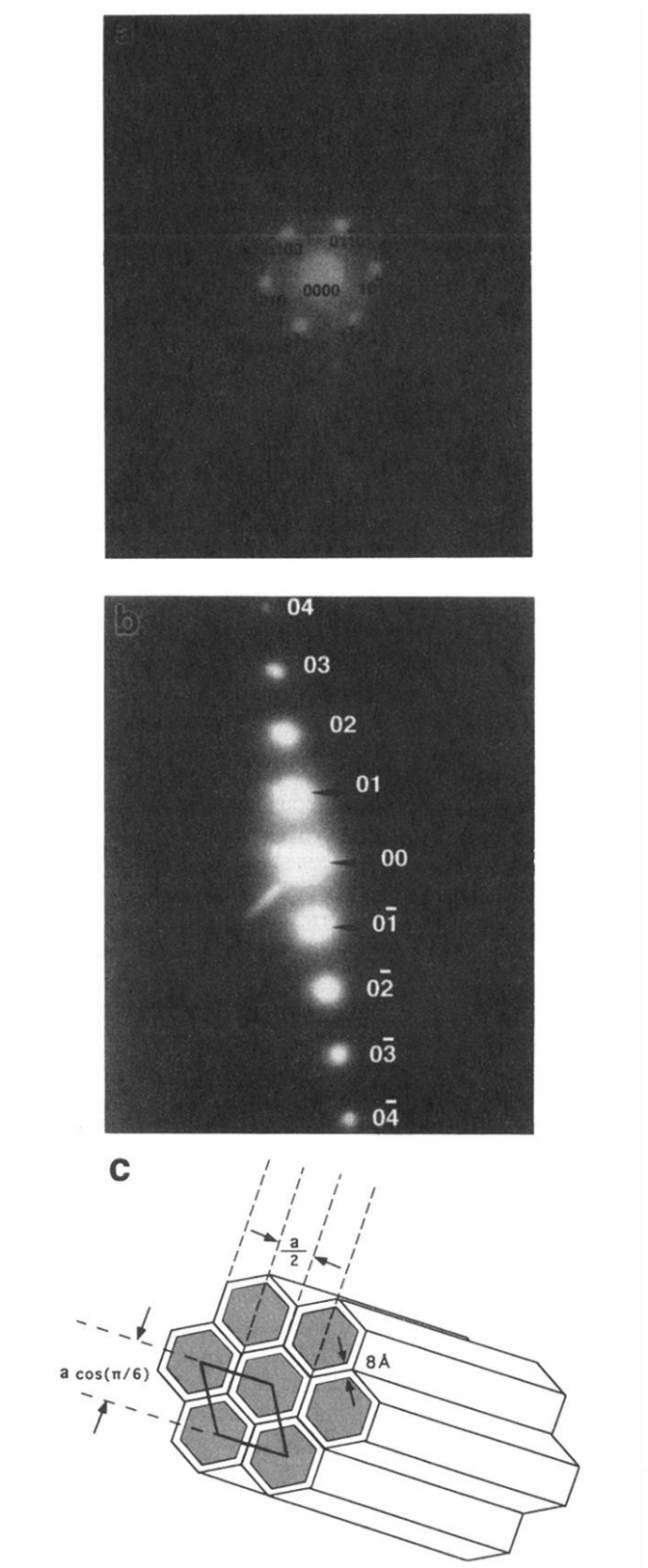

FIG. 1. Diffraction spots obtained from the mesosilicate MCM-41 used as host structure for Ge nanocrystals. The indexed diffraction pattern obtained (a) along the (0001) zone axis, and (b) normal to the hexagonal axis and parallel to two of the hexagonal tube side walls, giving d spacing of $a/2=25$ Å. (c) Diagram of an MCM-41 crystallite showing the different possible orientations that produce the lattice images shown in Figs. 4–6, as well as the diffraction patterns shown in (a) and (b).

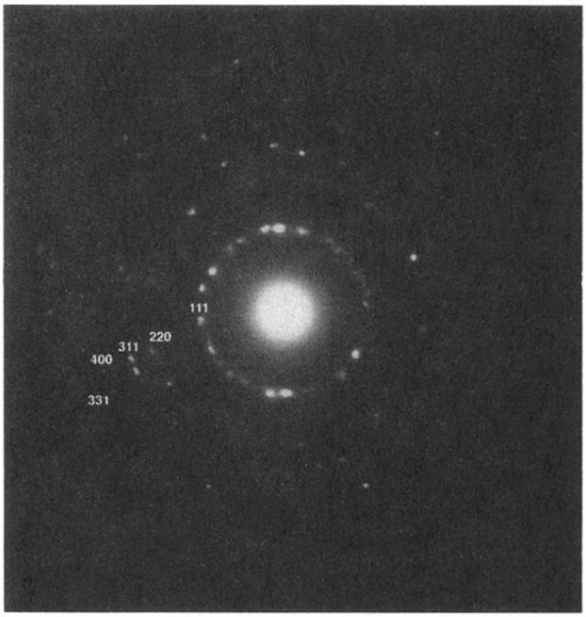

FIG. 3. Diffraction ring pattern obtained from Ge nanocrystals at several orientations in the MCM-41 framework. For randomly oriented particles and a specific beam direction, (hkl) diffracted beams will lie in a cone centered on the incident-beam direction producing a series of concentric rings each one corresponding to a set of $\{hkl\}$ reflections, as indexed here. The diffraction spots from the mesopore cannot be resolved from the transmitted beam in this figure.

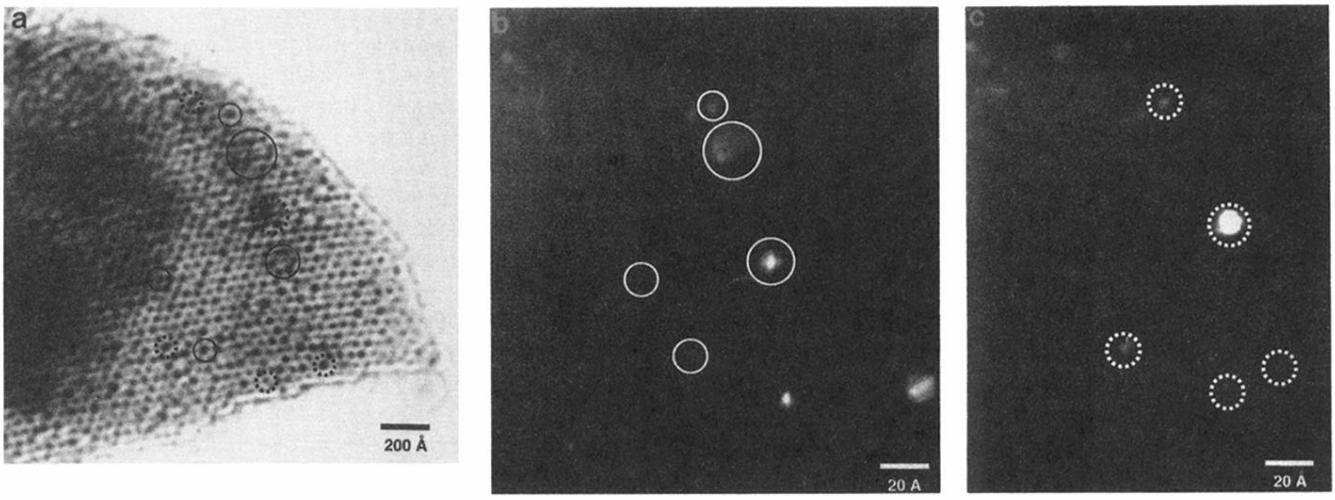

FIG. 4. (a) Phase contrast TEM micrograph obtained in axial bright-field imaging conditions shows the hexagonal framework of MCM-41. The Ge can be seen in some of the pores showing darker contrast due to stronger diffraction of the Ge crystals. (b) and (c) show axial dark-field images exhibiting contrast solely from Ge reflections chosen with two positions for the objective aperture (with some amorphous space included). The indicators show the corresponding places for the different imaging conditions.

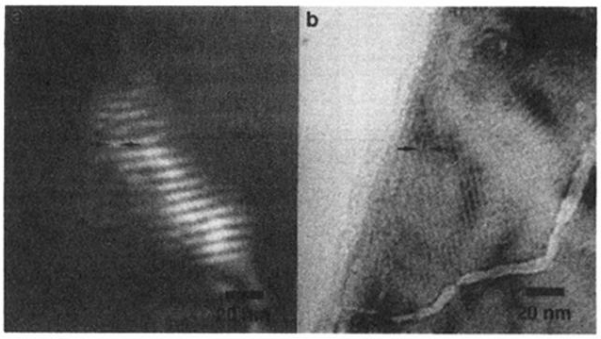

FIG. 5. (a) Dark field TEM micrograph where contrast is enanced due to moiré fringes. The smaller MCM-41 d-spacing in this orientation (25 Å) can also be seen normal to the larger moiré fringes. (b) Bright-field TEM micrograph of the same area as (a).